Self-sustained activity of low firing rate in balanced networks

F.S. Borges [a,*], P.R. Protachevicz [b], R.F.O. Pena [c], E.L. Lameu [d,e], G.S.V. Higa [a], A.H. Kihara [a], F.S. Matias [f,g], C.G. Antonopoulos [h], R. de Pasquale [i], A.C. Roque [c], K.C. Iarosz [j], P. Ji [k,l], A.M. Batista [b,m]

[a] Center for Mathematics, Computation, and Cognition, Federal University of ABC, São Bernardo do Campo, SP, Brazil
[b] Graduate in Science Program - Physics, State University of Ponta Grossa, PR, Brazil
[c] Laboratory of Neural Systems, Department of Physics, University of São Paulo, Ribeirão Preto, SP, Brazil
[d] National Institute for Space Research, São José dos Campos, SP, Brazil
[e] Department of Physics, Humboldt University, Berlin, Germany
[f] Institute of Physics, Federal University of Alagoas, Maceió, AL, Brazil
[g] Cognitive Neuroimaging Unit, CEA DRF/I2BM, INSERM, Université Paris-Sud, Université Paris-Saclay, F-91191 Gif/Yvette, France
[h] Department of Mathematical Sciences, University of Essex, Wivenhoe Park, UK
[i] Department of Physiology and Biophysics, ICB, University of São Paulo, São Paulo, SP, Brazil
[j] Institute of Physics, University of São Paulo, São Paulo, SP, Brazil
[k] Key Laboratory of Computational Neuroscience and Brain-Inspired Intelligence (Fudan University), Ministry of Education, China
[l] Institute of Science and Technology for Brain-Inspired Intelligence, Fudan University, Shanghai, China
[m] Department of Mathematics and Statistics, State University of Ponta Grossa, Ponta Grossa, PR, Brazil

ARTICLE INFO

ABSTRACT

Self-sustained activity in the brain is observed in the absence of external stimuli and contributes to signal propagation, neural coding, and dynamic stability. It also plays an important role in cognitive processes. In this work, by means of studying intracellular recordings from CA1 neurons in rats and results from numerical simulations, we demonstrate that self-sustained activity presents high variability of patterns, such as low neural firing rates and activity in the form of small-bursts in distinct neurons. In our numerical simulations, we consider random networks composed of coupled, adaptive exponential integrate-and-fire neurons. The neural dynamics in the random networks simulates regular spiking (excitatory) and fast spiking (inhibitory) neurons. We show that both the connection probability and network size are fundamental properties that give rise to self-sustained activity in qualitative agreement with our experimental results. Finally, we provide a more detailed description of self-sustained activity in terms of lifetime distributions, synaptic conductances, and synaptic currents.

© 2019 Published by Elsevier B.V.

1. Introduction

Self-sustained activity (SSA), where neurons display persistent activity even in the absence of external stimuli [1,2], is observed in diverse situations such as in *in vitro* cortical cultures and in slice preparations [3–5], in *in vivo* cortical preparations [6], in slow-wave sleep [7], in anesthesia [8], and in the resting state [9,10]. Electrophysiological recordings of SSA states show irregular neural spiking, typically with low average frequencies of a few Hertz, obeying long-tailed distributions [11–13].

---

* Corresponding author.
   E-mail addresses: fernandodasilvaborges@gmail.com (F.S. Borges), protachevicz@gmail.com (P.R. Protachevicz).

Many works have modelled neural networks with SSA by using random networks composed of excitatory and inhibitory leaky, integrate-and-fire (LIF) neurons with external background input [14–19]. Other studies have considered networks with non-random architectures, composed of LIF neurons [20–24] or nonlinear, two-dimensional integrate-and-fire neuron models [25–30]. Both the architecture and neuron types that comprise the network play an important role in SSA states. Such states are generated and maintained by recurrent interactions within networks of excitatory and inhibitory neurons. A stable SSA state is related to strong recurrent excitation within the neural network, which is restrained by inhibition to prevent runaway excitation. The balance between excitation and inhibition in neural networks is considered critical to maintain a SSA state [5,14,31–34]. Kumar et al. [17] studied the effects of network size on SSA states. Barak and Tsodyks [35] shown that combinations of synaptic depression and facilitation result in different network dynamics. Triplett et al. [36] analysed spontaneous activity in developing neural networks and shown that networks of binary threshold neurons can form structured patterns of neural activity.

In this work, we verify the existence of SSA in a random network composed of neurons with different intrinsic firing patterns (the so-called electrophysiological classes [37]). We consider the adaptive, exponential integrate-and-fire (AdEx) [38] model with cortical neurons modelled as regular spiking (RS) cells with spike frequency adaptation and fast-spiking (FS) cells with a negligible level of adaptation. In such networks, depending on the excitatory synaptic strength, neurons can exhibit a transition from spiking to bursting synchronisation [39,40] and bistable firing patterns [41]. We find conditions in which unstructured, sparsely connected random networks of AdEx neurons can display low frequency, self-sustained activity.

In particular, we show that not only the balance between excitation and inhibition but also the connection density and network size are both important factors for low frequency SSA. In balanced networks, high mean node-degree connectivity is necessary to give rise to low mean neural firing rates, and for such high values, large networks are necessary to support SSA states. In our computer simulations, we obtain qualitatively similar results to the ones we observed in our experimental recordings, where we use CA1 neurons whole-cell recordings in rats to demonstrate the possible variability of firing rate patterns observed in the brain. Our intracellular recordings show high variability of spontaneous activity patterns including low and irregular neural firing rates of approximately 1 Hz and spike-train power spectra with slow fluctuations [23], and small-bursts activity in distinct recorded neurons. Interestingly, we show that these results can be reproduced qualitatively by our model with cortical neurons modelled as regular spiking (RS) cells with spike frequency adaptation and fast-spiking (FS) cells with a negligible level of adaptation.

The paper is organised as follows: in Section 2, we introduce the neural network model and in Section 3, the various quantities used to study self-sustained activity in our numerical simulations and the details of our electrophysiological experiments. In Section 4, we present our results on self-sustained activity in the numerical simulations and experimental data, and in the last section we discuss them and draw our conclusions.

2. Neural network model

We start by building a random neural network of N AdEx neurons by connecting them with probability p, where p is the probability that any two neurons in the network are connected, excluding autapses (i.e. neurons connected to themselves, thus self-loops are not allowed). The N neurons are split into excitatory and inhibitory neurons according to the ratio 4:1 (meaning that 80% are excitatory and 20% are inhibitory), following [42]. The connection probability p and the mean connection degree K are associated by means of the relation

$$p = \frac{K}{N-1}. \tag{1}$$

The dynamics of each AdEx neuron $i = 1, \ldots, N$ in the network is given by the system of coupled equations [27]

$$C\frac{dV_i}{dt} = -g_L(V_i - E_L) + g_L \Delta_T \exp\left(\frac{V_i - V_T}{\Delta_T}\right) - \frac{1}{S}\left(w_i + \sum_{j=1}^{N} g_{ij}(V_i - E_j) + \Gamma_i\right), \tag{2}$$

$$\tau_w \frac{dw_i}{dt} = a(V_i - E_L) - w_i, \tag{3}$$

where V_i and w_i are, respectively, the membrane potential and adaptation current of neuron i, g_{ij} the synaptic conductance of the synapse from neuron j to neuron i, and Γ_i the external perturbation applied to neuron i. The synaptic conductance g_{ij} has exponential decay with synaptic time-constant τ_s. The parameter values in Eqs. (2) and (3) are given in Table 1. These values have been chosen so that the system can reproduce the spiking characteristics of RS (excitatory) and FS (inhibitory) neurons observed in experiments with real neurons [27].

When the membrane potential of neuron i is above a threshold potential ($V_i(t) > V_{\text{thres}} = -30$ mV), the neuron is assumed to generate a spike and the following update conditions are applied

$$V_i \rightarrow V_r = -60\,\text{mV}, \tag{4}$$

$$w_i \rightarrow w_i + b, \tag{5}$$

$$g_{ji} \rightarrow g_{ji} + g_s, \tag{6}$$

Table 1
Parameter values used in Eqs. (2) and (3). The ranges, where applicable, are indicated by square brackets. These values have been chosen so that the system of Eqs. (2) and (3) reproduces the spiking characteristics of RS (excitatory) and FS (inhibitory) neurons observed in experiments with real neurons [27].

Parameter	Symbol	Value
Membrane capacitance	C	1 μF/cm^2
Resting leak conductance	g_L	0.05 mS/cm^2
Resting potential	E_L	−60 mV
Slope factor	Δ_T	2.5 mV
Spike threshold	V_T	−50 mV
Membrane area	S	20,000 μm^2
Refractory time period	t_r	2.5 ms
Adaptation intensity	a	0.001 μS
Adaptation time constant	τ_w	600 ms
Integration time step	h	0.01 ms
Time	t	[0,10] s
Reversal potential	E_j	0 mV[a]
		−80 mV[b]
Synaptic time constant	τ_s	5 ms[a]
		10 ms[b]
Synaptic conductance	$g_s = g_{ex}$	[0,12] nS[a]
	$g_s = g_{in}$	[0,240] nS[b]
Synaptic delay	d	1.5 ms[a]
		0.8 ms[b]

[a]Indicates values for excitatory neurons.
[b]Indicates values for inhibitory neurons.

where V_r is the reset potential. Parameters b and g_s have different values depending on whether the neuron is excitatory or inhibitory: For excitatory neurons, $b = 0.01$ nA and $g_s = g_{ex}$, and for inhibitory neurons, $b = 0$ and $g_s = g_{in}$. Updates have synaptic delays of 1.5 ms and 0.8 ms for excitatory and inhibitory synapses, respectively. After the update, g_{ji} decays exponentially with a fixed time-constant τ_s (5 ms for excitatory and 10 ms for inhibitory synapses [22]). We define the relative inhibitory conductance g by

$$g = g_{in}/g_{ex} \tag{7}$$

as the parameter we will use in the investigation of network dynamics. In each simulation, we apply external stimuli Γ to 5% of the N neurons (randomly chosen) for 50 ms to initiate network activity, and then stop the external stimuli to observe the activity triggered, which can be persistent (SSA) or transient. For each neuron i, the external stimulus Γ_i has the same characteristics: it consists of excitatory current pulses with synaptic conductances that rise instantaneously to 0.01 μS and decay exponentially afterwards with a decay time of 5 ms, generated by a homogeneous Poisson process with rate 400 Hz.

All numerical simulations were implemented in C and the ordinary differential equations were integrated using the fourth order Runge–Kutta method with a fixed time step of $h = 0.01$ ms.

3. Quantities for the study of self-sustained activity in numerical simulations and details of electrophysiological experiments

In this work, we use the following mathematical quantities to study SSA based either on time intervals or specific spike timings.

3.1. Coefficient of variation

The coefficient of variation is defined based on time intervals and exploits the interspike interval (ISI) where the mth interval is defined as the difference between two consecutive spike-timings t_i^m and t_i^{m+1} of neuron i, namely $\text{ISI}_i = t_i^{m+1} - t_i^m > 0$. The coefficient of variation of the ith neuron is then given by

$$CV_i = \frac{\sigma_{\text{ISI}_i}}{\overline{\text{ISI}_i}}, \tag{8}$$

where σ_{ISI_i} is the standard deviation of the interspike intervals of neuron i.

3.2. Time-varying and mean network firing rates

We define the spike-train of neuron i as the sum of delta functions [43]

$$x_i(t) = \sum_{[t_i^m]} \delta(t - t_i^m), \tag{9}$$

where $[t_i^m]$ is the set of all spike-timings of neuron i for $t \in [0, T]$ and T the final integration time. Based on Eq. (9), we calculate the mean firing rate of neuron i over the time interval $[0, T]$ as

$$\bar{F}_i = \frac{1}{T} \int_0^T x_i(t)dt. \tag{10}$$

For all neurons in the network, we define the time-varying network firing rate (in Hz) in intervals of $\psi = 1$ ms as

$$F(t) = \frac{1}{\psi N} \sum_{i=1}^N \left(\int_t^{t+\psi} \delta(t - t_i^m)dt \right), \tag{11}$$

and the mean network firing rate over the time interval $[0, T]$ as

$$\bar{F} = \frac{1}{\langle \text{ISI} \rangle}, \tag{12}$$

where $\langle \text{ISI} \rangle$ is the mean ISI of the network given by

$$\langle \text{ISI} \rangle = \frac{1}{N} \sum_{i=1}^N \langle \text{ISI}_i \rangle. \tag{13}$$

3.3. Power spectrum, Fano factors and mean firing rate

Based on the definition of spike-trains $x_i(t)$ in Eq. (9), we define the power spectrum of neuron i as

$$S_i^{xx}(f) = \frac{\langle \tilde{x}_i(f)\tilde{x}_i^*(f) \rangle}{T}, \tag{14}$$

where $\langle \cdot \rangle$ indicates ensemble average, T is the final integration time, $\tilde{x}_i(f)$ is the Fourier transform of neuron i, given by

$$\tilde{x}_i(f) = \int_0^T e^{2\pi i f t} x_i(t)dt, \tag{15}$$

and $\tilde{x}_i^*(f)$ is the complex conjugate of $\tilde{x}_i(f)$. The power spectrum of a set of M ($M \leq N$) neurons, $\bar{S}^{xx}(f)$ is then defined as the average power spectrum of the M neurons

$$\bar{S}^{xx}(f) = \frac{1}{M} \sum_{i=1}^M S_i^{xx}(f). \tag{16}$$

To obtain consistent results over different simulations (see Fig. 5), we have chosen $M = 5 \times 10^4$, independently of N and K. In this work, we will use two quantities related to $\bar{S}^{xx}$ to describe spike-train characteristics [44–47].

The first quantity is the Fano factor $FF = \langle (n - \langle n \rangle)^2 \rangle / \langle n \rangle = \langle (\Delta n)^2 \rangle / \langle n \rangle$, which is defined as the ratio of the variance of n to the mean of the averaged spike count of the M neurons over the time window $[0, T]$, namely

$$n = \frac{1}{M} \sum_{i=1}^M \int_0^T x_i(t)dt. \tag{17}$$

Its relation to $\bar{S}^{xx}$ is meaningful in the vanishing frequency limit of $\bar{S}^{xx}(f)$, i.e. $\lim_{f \to 0} \bar{S}^{xx}(f) = \bar{F} \cdot FF$. The Fano factor, FF, is a standard measure of neural variability ($FF = 1$ corresponds to a Poisson process) and is related to the CV of the ISIs of the M neurons [48] by $\lim_{f \to 0} \bar{S}^{xx}(f) = \bar{F} \cdot \text{CV}^2 \left(1 + 2\sum_{k=1}^\infty r_k\right)$, where r_k is the serial correlation coefficient between ISIs that are lagged by k.

The second quantity is the mean firing rate of the M neurons, $\bar{F}_M$ (defined as in Eq. (12) but dividing by M), which is related to $\bar{S}^{xx}(f)$ by

$$\bar{F}_M = \lim_{f \to \infty} \bar{S}^{xx}(f). \tag{18}$$

3.4. Synaptic input

The instantaneous synaptic conductance of neuron i due to all excitatory and inhibitory synapses arriving to it, is denoted by

$$G_i(t) = \sum_{j \in \mathfrak{E}} g_{ij}(t) + \sum_{j \in \mathfrak{I}} g_{ij}(t) = G_{\text{ex},i}(t) + G_{\text{in},i}(t), \tag{19}$$

where $\mathfrak{E}$ and $\mathfrak{I}$ are the sets of all excitatory and inhibitory neurons in the network, respectively.

The instantaneous synaptic input to neuron i is then defined by

$$\begin{aligned} I_{\text{syn},i}(t) &= \sum_{j \in \mathfrak{E}} g_{ij}(E_j - V_i) + \sum_{j \in \mathfrak{I}} g_{ij}(E_j - V_i) \\ &= I_{\text{syn},i}^{\text{E}}(t) + I_{\text{syn},i}^{\text{I}}(t), \end{aligned} \tag{20}$$

and the mean synaptic input $\bar{I}_{\text{syn}}$ over all neurons in the network and over the simulation time in $[0, T]$ by

$$\bar{I}_{\text{syn}} = \frac{1}{N} \sum_{i=1}^{N} \frac{1}{T} \int_{t=0}^{T} \left(I_{\text{syn},i}^{\text{E}}(t) + I_{\text{syn},i}^{\text{I}}(t) \right) dt. \tag{21}$$

3.5. Mean network decay-time

Finally, for a given neuron i, we define the time of its last spike as the maximum time in its spike train,

$$t_i^{\text{last}} = \max \{t_i^m\}. \tag{22}$$

The network decay-time (DT) is then defined by the maximum of the last spikes of all neurons in the network during the simulation time, i.e. the maximum t_i^{last} of all neurons in the network,

$$\text{DT} = \max \{t_i^{\text{last}}, \ i = 1, \ldots, N\}. \tag{23}$$

Finally, we define the mean network decay-time $\overline{\text{DT}}$ as the mean DT over 10^3 simulations with different random initial conditions.

3.6. Details of electrophysiological experiments

3.6.1. Animals

Electrophysiological experiments were conducted using male Wistar rats with 20–25 postnatal days. All animals were kept in an animal facility in a 12:12 h light–dark cycle at a temperature of 23 °C $\pm$ 2° with free access to food and water. All procedures were approved by the Institutional Animal Care Committee of the Institute of Biomedical Sciences, University of São Paulo (CEUA ICB/USP n. 090, fls. 1°).

3.6.2. Preparation of brain slices

After animals were deeply anesthetised through isoflurane inhalation (AErrane; Baxter Pharmaceuticals), they were decapitated and the brain was quickly removed and submerged in cooled (0 °C) oxygenated (5% CO_2–95% O_2) cutting solution (in mM): 206 sucrose, 25 $NaHCO_3$, 2.5 KCl, 10 $MgSO_4$, 1.25 NaH_2PO_4, 0.5 $CaCl_2$, and 11 D-glucose. After removing the cerebellum, brain hemispheres were separated by a single sagittal cut. Both brain hemispheres were trimmed up and glued in a metal platform and sectioned using a vibratome (Leica - VT1200). 350–400 μm brain slices were obtained by advancing the vibratome blade from anterior–posterior orientation. Slices were rapidly transferred to a holding chamber containing artificial cerebrospinal fluid (ACSF; in mM): 125 NaCl, 25 $NaHCO_3$, 3 KCl, 1.25 NaH_2PO_4, 1 $MgCl_2$, 2 $CaCl_2$, and 25 D-glucose. Slices were kept oxygenated at room temperature (20–25°) for at least one hour before proceeding with electrophysiological recordings.

3.6.3. Electrophysiological recordings

Brain slices containing the hippocampal formation were placed in a submersion-type recording chamber upon a modified microscope stage and maintained at 30 °C with constant perfusion of oxygenated ACSF (5% CO_2–95% O_2). Whole-cell recordings were made from neurons located in the pyramidal layer of CA1. Recording pipettes were fabricated from borosilicate glass (Garner Glass) with input resistances of about 4–6 MΩ and were filled with intracellular solution (in mM): 135 K-gluconate, 7 NaCl, 10 HEPES, 2 Na2ATP, 0.3 Na3GTP, 2 $MgCl_2$; at a pH of 7.3 obtained with KOH and osmolality of 290 mOsm. All experiments were performed using a visualised slice setup under a differential interference contrast-equipped Nikon Eclipse E600FN microscope. Recordings were made using a Multiclamp 700B amplifier and pClamp software (Axon Instruments). Only recordings from cells that presented spontaneous activity with membrane potentials lower than −60 mV, access resistance lower than 20 MΩ, and input resistance higher than 100 MΩ and lower than 1000 MΩ, were included in our data. We injected depolarising currents to identify regular, tonic, or bursting spike patterns and neural spontaneous activity was assessed by 10 min of continuous recordings in current clamp mode.
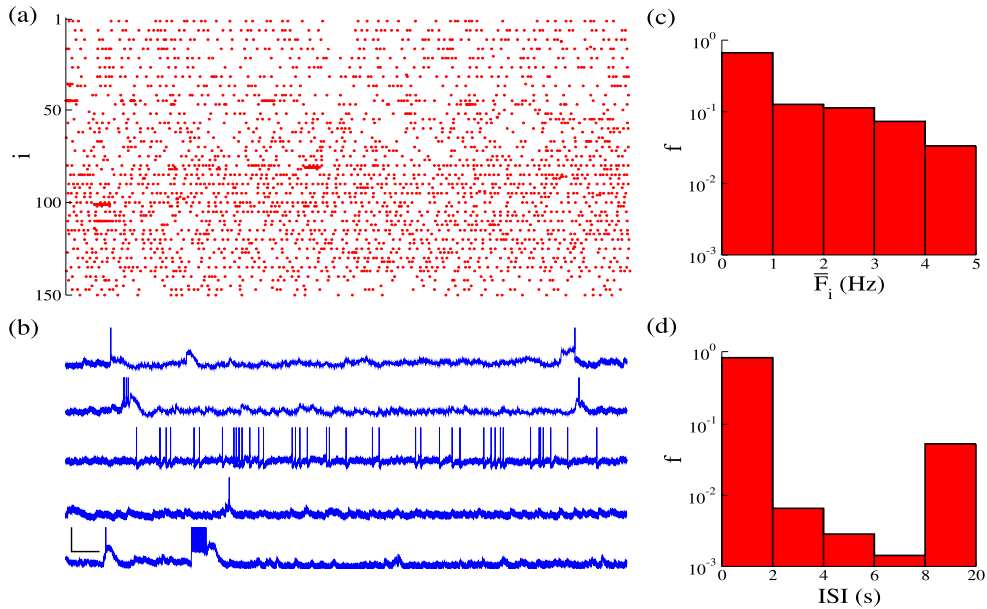
Fig. 1. Results from electrophysiological experimental data. (a) Raster plot of 150 traces. (b) Twenty seconds of recordings are shown (horizontal black bar denotes 1 s and vertical black bar denotes 50 mV). (c) Mean firing rate and (d) interspike interval (ISI) distributions. Note that the vertical axes in (c) and (d) are in logarithmic scale and that the label f represents the fraction of values in the bins in the horizontal axes.

4. Self-sustained activity

4.1. Self-sustained activity in electrophysiological experiments

SSA assessed by electrophysiological recordings in physiological brain states is characterised by irregular neural spiking, normally with low average frequency where rates follow a long-tailed distribution across neurons [23]. Interestingly, some brain regions are able to produce spontaneous network activity after a slicing procedure, including hippocampal sharp waves [49–51]. Once hippocampal slices present SSA manifested by spontaneous activity, we use CA1 neurons whole-cell recordings to demonstrate the possible variability of firing rate patterns observed in the brain. Our intracellular recordings show a high variability of spontaneous activity patterns including low neural firing rates and small-bursts activity in distinct recorded neurons.

Fig. 1 shows a representation of traces obtained by whole-cell patch clamp from CA1 neurons during a period of 20 s. The raster plot of the 150 traces is shown in Fig. 1(a), and five traces of membrane potential are shown in Fig. 1(b) for the same time window. The mean firing rate and interspike interval (ISI) distributions are plotted in Fig. 1(c) and (d), respectively. Recorded neurons present distinct firing patterns, including very low firing rate and small bursts of spikes, as shown in Fig. 1(b). In the whole record, the mean firing rate over all neurons is approximately equal to 1.172 Hz. Similar firing patterns, with high variability and low neural firing rates, are found in different recordings in the hippocampus and other cortices of the rat brain during slow-wave sleep [52], as well as in recordings from human middle temporal gyrus during sleep [53].

4.2. Self-sustained activity in numerical simulations

Here, we use the results from numerical simulations of a random network model of N adaptive exponential integrate-and-fire neurons [54] (Eqs. (2) and (3)). We focus on reproducing three aspects of the previous subsection (electrophysiological experimental data): (i) mean firing rates around 1 Hz, (ii) small-bursts activity in distinct neurons (Fig. 1(b)) and (iii) data with variability in firing rates where most of the neurons have frequencies between 0 and 1 Hz (Fig. 1(c)).

The random network model of N adaptive, exponential integrate-and-fire neurons [54] we use here is composed of 80% excitatory and 20% inhibitory neurons (i.e. a ratio of 4:1) following [42]. The synaptic conductance shows an exponential decay with synaptic delays of 1.5 ms and 0.8 ms for excitatory and inhibitory synapses, respectively. In each simulation, we apply external stimuli Γ to 5% of the N neurons (randomly chosen) for 50 ms to initiate network activity. Then, we stop the external stimulation to observe the activity triggered, which can be persistent (i.e. SSA) or transient.

To reproduce SSA firing patterns with low neural firing rates, we analyse the parameter space $g_{ex} \times g$ for a neural, random, network of $N = 10^4$ AdEx neurons with connection probability $p = 0.02$. We focus on an area of the parameter space where there is a balanced regime of excitation and inhibition. In this area, we do not observe SSA for $g_{ex} < 0.004\,\mu S$,
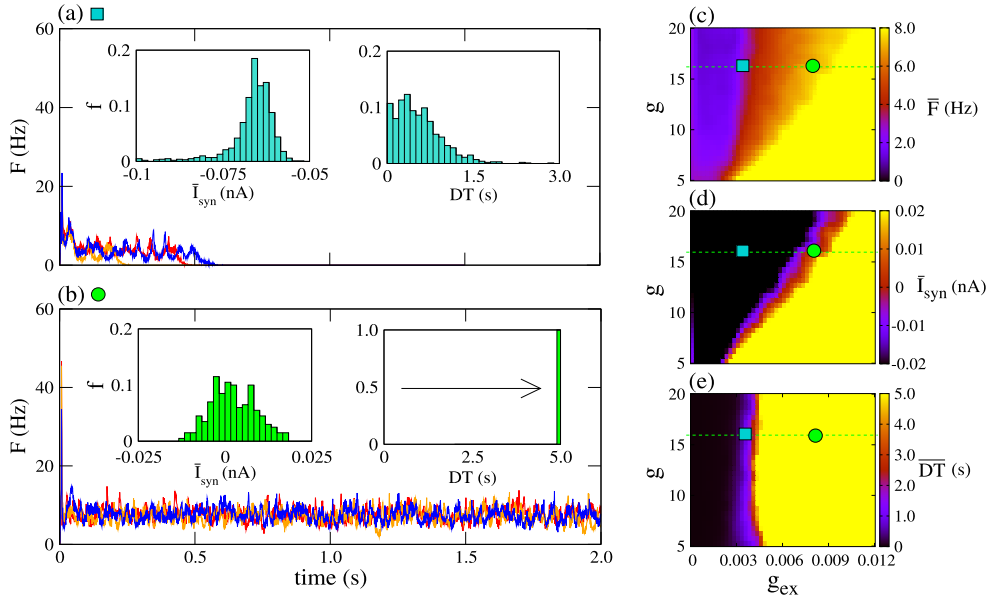
Fig. 2. Results from the numerically simulated data. Time-dependent network firing rate (F) in two distinct regimes: (a) non-SSA and (b) SSA. Each case corresponds to a different simulation. The two neural network models use the same set of parameters except that the excitatory conductance is $g_{ex} = 0.0035$ μS in (a) and $g_{ex} = 0.008$ μS in (b). The insets show the probability distribution of the mean synaptic inputs ($\bar{I}_{syn}$) over 10^3 simulations and decay-times (DT) in each case. (c) Mean network firing rate ($\bar{F}$), (d) mean synaptic input ($\bar{I}_{syn}$) and (e) Mean decay-time ($\overline{DT}$) as a function of excitatory (g_{ex}) and relative inhibitory synaptic coupling (g). The neural network has $N = 10^4$ neurons and the connection probability is $p = 0.02$. In (a) and (b), we fixed $g = 16$. The turquoise squares correspond to the parameters in (a) and the green circles to those in (b). Note that the label f in the insets in (a) and (b) represents the fraction of values in the bins in the horizontal axes.

i.e. in the weak coupling region. Examples of time-dependent network firing rates in this region are shown in Fig. 2(a), for $g_{ex} = 0.0035$ μS and $g = 16$. The initial stimulus applied in the first 50 ms, generates short-lived activity in the network. The mean synaptic input, $\bar{I}_{syn}$, is negative (left-hand inset in Fig. 2(a)) and the network decay-time DT is always less than 3 s (right-hand inset in Fig. 2(a)). Examples of time-dependent network firing rates in the region of SSA are shown in Fig. 2(b), corresponding to $g_{ex} = 0.008$ μS and $g = 16$. The mean synaptic input is approximately balanced ($\bar{I}_{syn} \approx 0$) and the decay-time is higher than the maximum time used in our simulations (i.e. DT ≥ 5 s).

For $N = 10^4$ neurons, the lowest mean network firing rates are approximately 2 Hz. The region where these rates occur is shown in purple in Fig. 2(c). A particular case for $g_{ex} < 0.0035$ μS is indicated by a turquoise square, where the activity is not self-sustained. For the random network and parameter space considered, the region with SSA is roughly determined by $g_{ex} > 0.004$ μS (indicated in yellow in Fig. 2(e)). The lowest mean network firing rate of an SSA state is around 4 Hz (red region in Fig. 2(c)). Within this region, one can identify the region of excitation/inhibition balance by considering the region with $I_{syn} \approx 0$ (see Eq. (21)). This is shown in red in Fig. 2(d). The black and yellow regions in Fig. 2(d) correspond to slightly predominant inhibitory and excitatory mean synaptic input, respectively. An SSA case with $\bar{F} \approx 4$ Hz and excitation/inhibition balance is indicated by the green circle in Fig. 2(c)–(e) and corresponds to $g_{ex} = 0.008$ μS and $g = 16$.

To study the effect of the size of the network on SSA, we considered two networks of different sizes with the same mean degree. The first has $N = 10^4$ and $p = 0.04$ and the second $N = 2 \times 10^4$ and $p = 0.02$, both having $K = 400$. The parameters ($g_{ex} = 0.005$ μS and $g = 8$) are the same for the two networks, and put them close to the balanced state. In Fig. 3(a), we show the firing rate evolution of the two networks. For $N = 10^4$ (turquoise line), the activity decays before 2 s, and for $N = 2 \times 10^4$ (green line) SSA is observed. The distributions of $\bar{I}_{syn}$ for the two cases (see the insets in Fig. 3(a)) have similar (positive) average values but the one for $N = 10^4$ is broader and left-skewed. The decay-time distribution (Fig. 3(b), (c)) clearly shows that the networks with $N = 2 \times 10^4$ have SSA, while the ones with $N = 10^4$ are predominantly short-lived. A comparison of networks with the two sizes in the $g_{ex} \times g$ parameter space is shown in Fig. 3(d)–(i). The mean network firing rate and mean synaptic input display similar behaviour in the parameter space for the two network sizes (Fig. 3(d)–(g)). However, this similarity is not seen in the diagram for $\overline{DT}$ (Fig. 3(h)–(i)). The region corresponding to SSA (yellow) is larger for $N = 2 \times 10^4$ than for $N = 10^4$. Moreover, the shape of this region for $N = 2 \times 10^4$ discloses almost absent sensitivity of SSA duration to the relative inhibitory synaptic conductance g. On the other hand, for $N = 10^4$, the SSA lifetime is sensitive to g for 0.006 μS $\lesssim g_{ex} \lesssim 0.008$ μS, and only for strong coupling ($g_{ex} \gtrsim 0.008$ μS), it becomes insensitive to g. In Fig. 3, we observe large decay time DT for high frequencies.

Next, we investigate the influence of N, p and K (see Eq. (1)) on the network firing rate of SSA states. We fix $g_{ex} = 0.008$ μS and $g = 16$ to keep the dynamics around an excitatory/inhibitory balance. Fig. 4 shows the mean network firing rate
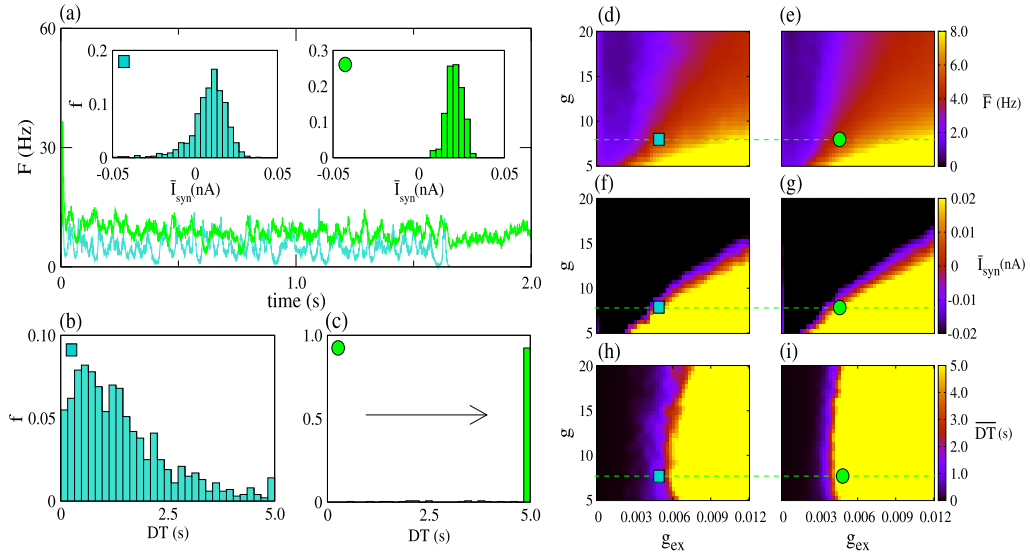
Fig. 3. Results from the numerically simulated data. (a) Time-dependent network firing rate (F) for $N = 10^4$ (turquoise line) and $N = 2 \times 10^4$ (green line). The insets show the probability distribution of the mean synaptic input ($\bar{I}_{syn}$) over 10^3 simulations, for each case. (b) and (c) show the decay-time (DT) distribution (also for 10^3 simulations) for $N = 10^4$ and $N = 2 \times 10^4$, respectively (colours follow the same convention as in (a)). We considered the excitatory conductance $g_{ex} = 0.005$ μS, mean node-degree $K = 400$, and relative inhibitory synaptic coupling $g = 8$. The mean network firing rates (d) and (e), mean synaptic inputs (f) and (g), and mean decay-times (h) and (i) are shown as a function of g_{ex} and g for $N = 10^4$ (left) and $N = 2 \times 10^4$ (right), respectively. The turquoise squares correspond to $N = 10^4$ and $p = 0.04$ and the green circles to $N = 2 \times 10^4$ and $p = 0.02$. Note that the label f in the insets in (a) and (b) represents the fraction of values in the bins in the horizontal axes.

of SSA states (colour scale) in the parameter space $N \times p$. The white area in the parameter space corresponds to non-SSA states. We can see that the mean network firing rate of SSA states depends on both N and p. In particular, low firing rate SSA states appear when the network size N increases. The black solid line in Fig. 4 represents networks with mean node-degree $K = 1500$, in which case there are SSA states for $N \geq 1.5 \times 10^5$ neurons. The inset in Fig. 4(a) shows the dependence of the mean network firing rate $\bar{F}$ of SSA states on the mean connection node-degree K for constant N. We can observe that lower rates are obtained for increased K. However, very low firing rates (≈ 1 Hz) are present only for very large network sizes. In the inset in Fig. 4(b), we can observe that the network size does not alter the mean network firing rate when K is fixed. Therefore, large K plays an important role in the occurrence of low network firing rates, and for such low firing rates, large-size networks are necessary to support SSA states.

Fig. 5 shows results for three cases of network sizes and mean node-degrees K, namely for $N = 10^5$ and $K = 1300$, for $N = 3 \times 10^5$ and $K = 1500$ and for $N = 5 \times 10^5$ and $K = 1700$. The time-varying network firing rate is non-periodic and its mean value decreases as both N and K increase (Fig. 5(a)). In Fig. 5(c)–(e), we observe that most ISIs are distributed in the interval [0, 2] s. These results agree with the experimental results in Fig. 1(d), where more than 60% of ISIs are in a similar interval. In the three cases, the spiking variability, characterised by the ISI distribution, is very well described by a Poisson distribution (Fig. 5(c)–(e)). This is characteristic of irregular neural firing [19,55–57]. Moreover, the CV of the ISIs slowly converges to the one of a Poisson process (= 1) as both N and K increase.

As discussed in Section 3, the power spectrum of a set of M neurons is related to different quantities that characterise network firing. In our numerical simulations, we can observe these relations by taking the limits of the power spectrum as $f \to \infty$ or $f \to 0$. The mean firing rate $\bar{F}_M$ is associated with the infinity frequency limit, namely $\lim_{f \to \infty} \bar{S}^{xx}(f) = \bar{F}_M$ (see also Eq. (18)). In Fig. 5(b), one can see that these mean firing rates are very low (1 Hz $\lesssim \bar{F}_M \lesssim$ 1.5 Hz) and that the smaller rates occur for larger N and K. On the other hand, irregularity is associated with vanishing frequency, namely $\lim_{f \to 0} \bar{S}^{xx}(f) = \bar{F}.FF$, where FF is the Fano factor (see Section 3.3). Assuming approximately the same $\bar{F}$ for the three networks in Fig. 5(b), say $\bar{F} \approx 1.3$, the $f \to 0$ limit of $\bar{S}^{xx}(f)$ shows that $FF > 1$ for all of them. This suggests a process more irregular than the Poisson process [58], e.g. bursting [56]. Moreover, as the network size N increases, FF decreases, indicating tendency to converge to a Poisson process and is linked to a standard irregularity measure and CV. We see that in the limit of very small frequencies, the value of the power spectra decreases as both K and N increases, confirming the behaviour observed by CV, i.e. the spiking times are becoming more regular. The power spectra display slow fluctuations, which can be explained by the low neural firing rates and bursting spiking patterns (as discussed below). Slow power spectrum fluctuations are also features of spontaneous activity in cortical networks [10,46,59].

In Fig. 6, we show characteristics of the SSA firing patterns with low rate exhibited by the network (a particular case with $N = 5 \times 10^5$ and $K = 1700$ is shown as a representative example). The patterns are characterised by sparse and non-synchronous activity (Fig. 6(a)), akin to what has been termed the heterogeneous variant [19] of the
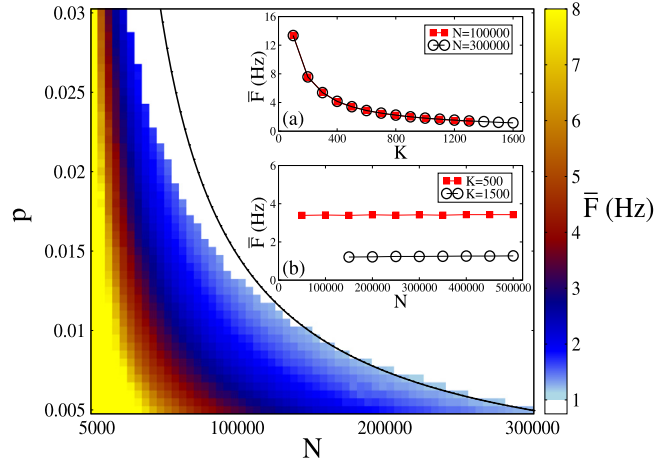
Fig. 4. Results from the numerically simulated data. Each point in the coloured part of the plot gives $\bar{F}$ calculated for a simulation with the corresponding parameter values of N and p. The white area corresponds to non-SSA states. The black line represents networks with mean node-degree $K = 1500$ (according to Eq. (1)). Upper inset: mean network firing rate $\bar{F}$ as a function of K, keeping N fixed, where the red squares and black circles represent $N = 10^5$ and $N = 3 \times 10^5$ neurons, respectively. Lower inset: mean network firing rate $\bar{F}$ as a function of N, showing independence of $\bar{F}$ on N for constant connection degree K. The curves represent two selected K values: $K = 500$ (red squares) and $K = 1500$ (black circles). Note that we have used $g_{ex} = 0.008$ μS and $g = 16$ for all simulations in this figure.
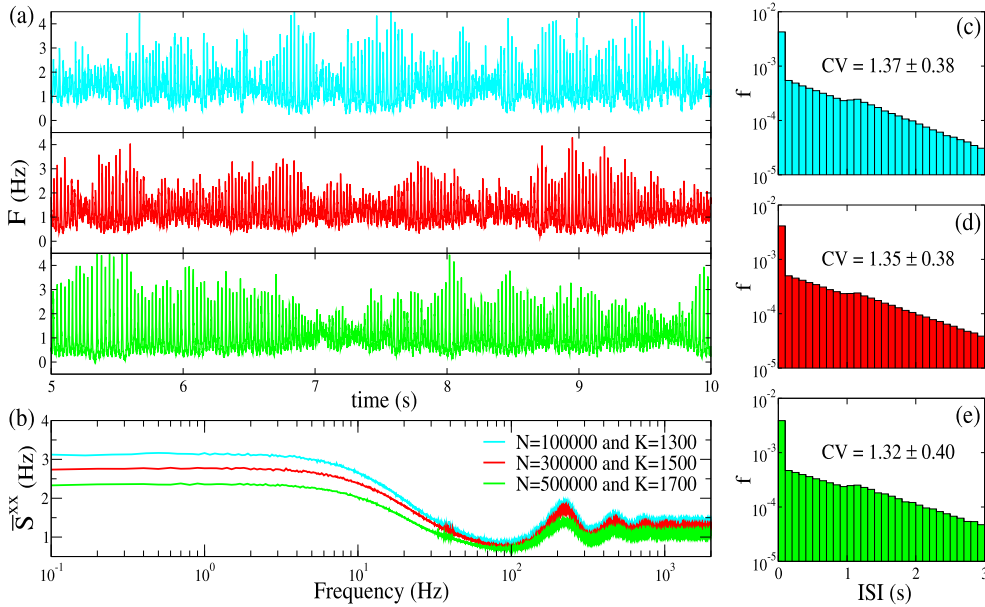

Fig. 5. Results from the numerically simulated data. (a) From top to bottom, we show F as N and K increase (for the N and K values, see legend in (b)). (b) Power spectra averaged over 5×10^4 neurons in the network and 10 s of simulation. Note that the horizontal axis is logarithmic and the vertical linear. (c)–(e) ISI distributions for the same three networks with the vertical axes in logarithmic and horizontal in linear scales. The values of the corresponding CVs are shown in the plots. In the three cases, the parameter values used are $g_{ex} = 0.008$ μS and $g = 16$. Note that the vertical axes in (c), (d) and (e) are in logarithmic scale and that the label f represents the fraction of values in the bins in the horizontal axes.

asynchronous irregular (AI) regime [14,60]. In the homogeneous AI regime, all neurons fire with the same mean rate, but in the heterogeneous AI regime, the mean firing rates fluctuate in time and across neurons. In some cases, neurons can even exhibit bursting periods (as can be seen in Fig. 6(b)). Neurons have low firing rates, with a right-skewed distribution that peaks around 1 Hz (Fig. 6(d)). Irregularity is confirmed by the CV of ISIs and power spectra analysis (Fig. 5). The similarity between the firing regime observed in our simulations and the heterogeneous AI state can be further verified by a comparison of the respective spike-train power spectra. Spectra for networks in heterogeneous AI have been calculated elsewhere [47] and display slow fluctuations as shown here (Fig. 5(b)).
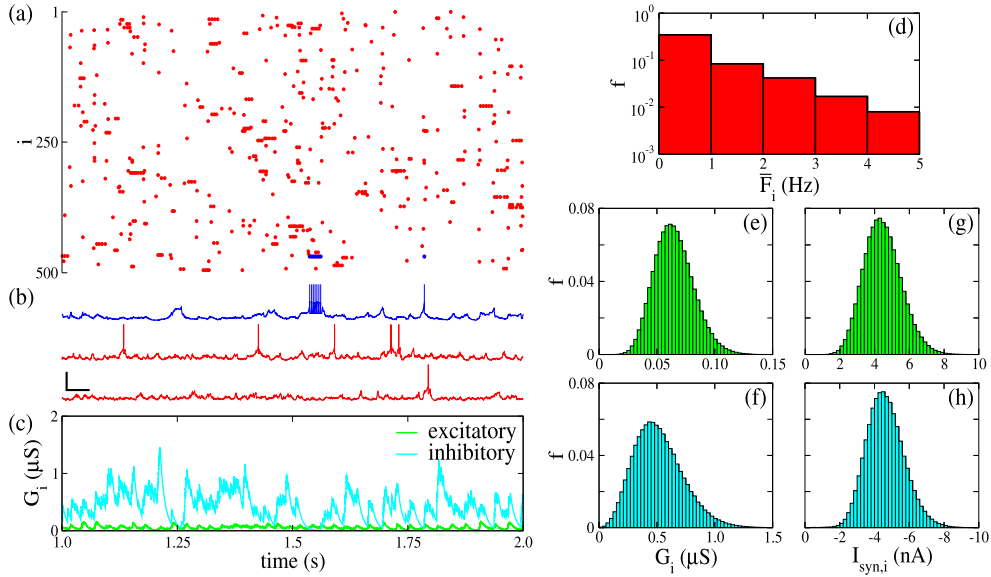
Fig. 6. Results from the numerically simulated data. All plots refer to a single simulation of a network with $N = 5 \times 10^5$, $K = 1700$, $g_{ex} = 0.008$ μS and $g = 16$. (a) Raster plot of 2 s of simulation time (only 500 randomly chosen neurons from the network are shown). (b) membrane potential of three randomly chosen neurons from the network (the horizontal black bar denotes 0.2 s and the vertical black bar denotes 50 mV). (c) Time-varying synaptic conductances ($G_{ex,i}(t)$ in green and $G_{in,i}(t)$ in cyan) of neurons represented by the blue line in (b). (d) distribution of mean firing rates $\bar{F}_i$ (Eq. (10)) of all neurons in the network. Distribution of excitatory ($G_{ex,i}$) (e) and inhibitory ($G_{in,i}$) (f) synaptic conductances of all neurons at the end of the simulation. Distribution of excitatory ($I^E_{syn,i}$) (g) and inhibitory ($I^I_{syn,i}$) (h) synaptic inputs of all network neurons at the end of the simulation. Note that the vertical axis in (d) is in logarithmic scale and that the label f in (d), (e), (g), (f) and (h) represents the fraction of values in the bins in the horizontal axes.

The distributions of the excitatory (G_{ex}) and inhibitory (G_{in}) synaptic conductances over neurons (panels (e) and (f) in Fig. 6) have nearly symmetric shapes, with the G_{in} distribution slightly right skewed, in agreement with experimental evidence [61], even though the conductance values per se are higher than in the experimental recordings. The distributions of excitatory (I^E_{syn}) and inhibitory (I^I_{syn}) synaptic inputs are nearly identical and vary over nearly the same range of absolute values, though the upper end of the range is slightly higher for the inhibitory synaptic inputs (see panels (g) and (h) in Fig. 6). This is a hallmark of a balanced state, and the neural spikes occur due to the large synaptic conductance variability, which allows for the necessary conditions that can support the appearance of SSA.

Finally, it is worthwhile the fact that in Fig. 6(a) (raster plot) and 6(b) (membrane potential), there are several striking similarities, namely: non-synchronous activity and, the coexistence of spike and bursting neural activity. More importantly though, qualitatively similar activities and behaviours are present in the data obtained from hippocampal slices (electrophysiological experiments) as demonstrated in Fig. 1(a)–(b) and in the results from the numerical simulations data. In both experimental and numerically simulated data, we observe high variability in neural firing rates where most of the neurons fire with frequencies in the interval [0, 1] Hz, with similar distribution of mean firing rates in the interval [1, 5] Hz (compare Figs. 1(c) and 6(d)).

5. Conclusions and discussion

In this paper, motivated by self-sustained activity observed in the brain in the absence of external stimuli, we sought to study necessary conditions for which irregular and low-frequency self-sustained dynamics emerge in models of neural networks with random connectivity. We build neural network models of 80% excitatory and 20% inhibitory neurons randomly connected and mathematically described by the adaptive, exponential integrate-and-fire model. This model mimics the behaviour of biological neurons, exhibiting spiking and bursting patterns of activity. We studied network features by varying: (i) the balance between excitation and inhibition in the system and (ii) the topological characteristics of the random network by means of varying the mean node-degree. Results were obtained by running a large number of numerical simulations to compute firing rates and related quantities, and compared them with results from our electrophysiological experiments using whole-cell patch clamp from CA1 rat neurons.

Our numerical results allowed us to observe neural activity with slow fluctuations in the absence of external perturbation. We found that the patterns of low firing-rate self-sustained activity is asynchronous and irregular as depicted in raster plots. We shown that the irregular spikes with low firing rate depend on the mean node degrees of the neurons, and that low-rate self-sustained activity occurs for a tight balance between inhibition/excitation and large network sizes. We found that for fixed mean connection degree, the mean network firing rate does not change with the network size.

In an excitation/inhibition balanced random network, if the network size is fixed, the mean network firing rate decreases when the mean node-degree increases. However, there is a maximum mean node-degree value for which it is possible to maintain self-sustained activity states, and this value is proportional to the network size. Therefore, large networks are necessary to give rise to self-sustained activity states when the mean node-degree is large. Moreover, the occurrence of spikes is due to the synaptic-conductance variability and the inhibitory synaptic input is slightly higher than the excitatory.

More importantly, we found that our results from the numerical simulations resemble those obtained from our experimental recordings and analysis, such as irregular firing with firing rates of about 1 Hz. In addition, we have demonstrated that our model is able to reproduce the coexistence of spike and bursting neurons and the distribution of mean firing rates between 0 and 5 Hz obtained by our electrophysiological experiments using whole-cell patch clamp from CA1 rat neurons.

Concluding, we have been able to demonstrate the existence of low neural firing rate self-sustained activity in excitation/inhibition balanced random networks of adaptive, exponential integrate-and-fire neurons. This phenomenon is characterised by irregular neural oscillations and shows that low frequency self-sustained activity can be found in large balanced random networks, a result that is qualitatively similar to those obtained from our electrophysiological experiments using whole-cell patch clamp from CA1 rat neurons.

Acknowledgments

References

[1] M.D. Greicius, B. Krasnow, A.L. Reiss, V. Menon, Functional connectivity in the resting brain: a network analysis of the default mode hypothesis, Proc. Natl. Acad. Sci. USA 100 (2003) 253.

[2] M.D. Fox, A.Z. Snyder, J.L. Vincent, M. Corbetta, D.C. Van Essen, M.E. Raichle, The human brain is intrinsically organized into dynamic, anticorrelated functional networks, Proc. Natl. Acad. Sci. USA 102 (2005) 9673.

[3] D. Plenz, A. Aertsen, Neural dynamics in cortex-striatum co-cultures II, Spatiotemporal characteristics of neural activity, Neuroscience 70 (1996) 893.

[4] M.V. Sanchez-Vives, D.A. McCormick, Cellular and network mechanisms of rhythmic recurrent activity in neocortex, Nature Neurosci. 10 (2000) 1027.

[5] Y. Shu, A. Hasenstaub, D.A. McCormick, Turning on and off recurrent balanced cortical activity, Nature 432 (2003) 288.

[6] I. Timofeev, F. Grenier, M. Bazhenov, T.J. Sejnowski, M. Steriade, Origin of slow cortical oscillations in deafferented cortical slabs, Cerebral Cortex 10 (2000) 1185.

[7] M. Steriade, I. Timofeev, F. Grenier, Natural waking and sleep states: a view from inside neocortical neurons, J. Neurophysiol. 85 (2001) 1969.

[8] M. Steriade, A. Nunez, F. Amzica, A novel slow (< 1 Hz) oscillation of neocortical neurons in vivo: depolarizing and hyperpolarizing components, J. Neurosci. 13 (1993) 3252.

[9] A. Arieli, D. Shoham, R. Hildesheim, A. Grinvald, Coherent spatiotemporal patterns of ongoing activity revealed by real-time optical imaging coupled with single-unit recording in the cat visual cortex, J. Neurophysiol. 73 (1995) 2072.

[10] D. Mantini, M.G. Perrucci, C. Del Gratta, G.L. Romani, M. Corbetta, Electrophysiological signatures of resting state networks in the human brain, Proc. Natl. Acad. Sci. USA 104 (2007) 13170.

[11] T. Hromádka, M.R. DeWeese, A.M. Zador, Sparse representation of sounds in the unanesthetized auditory cortex, PLoS Biol. 6 (2008) 0124.

[12] D.H. O'Connor, S.P. Peron, D. Huber, K. Svoboda, Neural activity in barrel cortex underlying vibrissa-based object localization in mice, Neuron 67 (2010) 1048.

[13] G. Buzsáki, K. Mizuseki, The log-dynamic brain: how skewed distributions affect network operations, Nat. Rev. Neurosci. 15 (2014) 264.

[14] N. Brunel, Dynamics of sparsely connected networks of excitatory and inhibitory spiking neurons, J. Comput. Neurosci. 8 (2000) 183.

[15] T.P. Vogels, L.F. Abbott, Signal propagation and logic gating in networks of integrate-and-fire neurons, J. Neurosci. 25 (2005) 10786.

[16] N. Parga, L.F. Abbott, Network model of spontaneous activity exhibiting synchronous transitions between up and down states, Front. Neurosci. 1 (2007) 57.

[17] A. Kumar, S. Schrader, A. Aertsen, S. Rotter, The high-conductance state of cortical networks, Neural Comput. 20 (2008) 1.

[18] B. Kriener, H. Enger, T. Tetzlaff, H.E. Plesser, M.-O. Gewaltig, G.T. Einevoll, Dynamics of self-sustained asynchronous irregular activity in random networks of spiking neurons with strong synapses, Front. Comput. Neurosci. 8 (2014) 1.

[19] S. Ostojic, Two types of asynchronous activity in networks of excitatory and inhibitory spiking neurons, Nature Neurosci. 17 (2014) 594.

[20] A. Renart, R. Moreno-Bote, X.-J. Wang, N. Parga, Mean-driven and fluctuation-driven persistent activity in recurrent networks, Neural Comput. 19 (2007) 1.

[21] M. Kaiser, C.C. Hilgetag, Optimal hierarchical modular topologies for producing limited sustained activation of neural networks, Front. Neuroinform. 4 (2010) 1.

[22] S.-J. Wang, C.C. Hilgetag, C. Zhou, Sustained activity in hierarchical modular neural networks: self-organized criticality and oscillations, Front. Comput. Neurosci. 5 (2011) 1.

[23] A. Litwin-Kumar, B. Doiron, Slow dynamics and high variability in balanced cortical networks with clustered connections, Nature Neurosci. 15 (2012) 1498.

[24] T.C. Potjans, M. Diesmann, The cell-type specific cortical microcircuit: relating structure and activity in a full-scale spiking network model, Cerebral Cortex 24 (2014) 785.

[25] A. Compte, Computational and in vitro studies of persistent activity: edging towards cellular and synaptic mechanisms of working memory, Neuroscience 139 (2006) 135.

[26] E.M. Izhikevich, G.M. Edelman, Large-scale model of mammalian thalamocortical systems, Proc. Natl. Acad. Sci. USA 105 (2008) 3593.

[27] A. Destexhe, Self-sustained asynchronous irregular states and up-down states in thalamic, cortical and thalamocortical networks of nonlinear integrate-and-fire neurons, J. Comput. Neurosci. 27 (2009) 493.

[28] P. Stratton, J. Wiles, Self-sustained non-periodic activity in networks of spiking neurons: The contribution of local and long-range connections and dynamic synapses, Neuroimage 52 (2010) 1070.

[29] P. Tomov, R.F. Pena, M.A. Zaks, A.C. Roque, Sustained oscillations, irregular firing, and chaotic dynamics in hierarchical modular networks with mixtures of electrophysiological cell types, Front. Comput. Neurosci. 8 (2014) 1.

[30] P. Tomov, R.F. Pena, A.C. Roque, M.A. Zaks, Mechanisms of self-sustained oscillatory states in hierarchical modular networks with mixtures of electrophysiological cell types, Front. Comput. Neurosci. 10 (2016) 1.

[31] C.A. van Vreeswijk, H. Sompolinsky, Chaos in neural networks with balanced excitatory and inhibitory activity, Science 274 (1996) 1724.

[32] B. Haider, A. Duque, A.R. Hasenstaub, D.A. McCormick, Neocortical network activity in vivo is generated through a dynamic balance of excitation and inhibition, J. Neurosci. 26 (2006) 4535.

[33] A.H. Taub, Y. Katz, I. Lampl, Cortical balance of excitation and inhibition is regulated by the rate of synaptic activity, J. Neurosci. 33 (2013) 14359.

[34] E. Nanou, A. Lee, W.A. Catterall, Control of excitation/inhibition balance in a hippocampal circuit by calcium sensor protein regulation of presynaptic calcium channels, J. Neurosci. 38 (2018) 4430.

[35] O. Barak, M. Tsodyks, Persistent activity in neural networks with dynamic synapses, PLoS Comput. Biol. 3 (2007) e35.

[36] M.A. Triplett, L. Avitan, G.J. Goodhill, Emergence of spontaneous assembly activity in developing neural networks without afferent input, PLoS Comput. Biol. 14 (2018) e1006421.

[37] D. Contreras, Electrophysiological classes of neocortical neurons, Neural Netw. 17 (2004) 633.

[38] R. Brette, W. Gerstner, Adaptive, exponential integrate-and-fire model as an effective description of neural activity, J. Neurophysiol. 94 (2005) 3637.

[39] F.S. Borges, P.R. Protachevicz, E.L. Lameu, R.C. Bonetti, K.C. Iarosz, I.L. Caldas, M.S. Baptista, A.M. Batista, Synchronised firing patterns in a random network of adaptive, exponential integrate-and-fire neuron model, Neural Netw. 90 (2017) 1.

[40] P.R. Protachevicz, R.R. Borges, A.S. Reis, F.S. Borges, K.C. Iarosz, I.L. Caldas, E.L. Lameu, E.E.M. Macau, R.L. Viana, I.M. Sokolov, F.A.S. Ferrari, J. Kurths, A.M. Batista, Synchronous behavior in network model based on human cortico-cortical connections, Physiol. Meas. 39 (2018) 1.

[41] P.R. Protachevicz, F.S. Borges, E.L. Lameu, P. Ji, K.C. Iarosz, A.H. Kihara, I.L. Caldas, J.D. Szezech Jr, M.S. Baptista, E.E.M. Macau, C.G. Antonopoulos, A.M. Batista, J. Kurths, Bistable firing pattern in a neural network model, Front. Comput. Neurosci. 13 (2019) 19.

[42] C.R. Noback, N.L. Strominger, R.J. Demarest, D.A. Ruggiero, The Human Nervous System: Structure and Function, sixth ed., Humana Press, Totowa, NJ, 2005.

[43] F. Gabbiani, C. Koch, Principles of spike train analysis, in: C. Koch, I. Segev (Eds.), Methods in Neural Modeling, MIT Press, Cambridge, 1998, p. 313.

[44] B. Lindner, A brief introduction to some simple stochastic processes, in: Stochastic Methods in Neuroscience, Oxford University Press, Oxford, 2009, p. 1.

[45] S. Grün, S. Rotter, Analysis of Parallel Spike Trains, Springer Science & Business Media, 2010, p. 1.

[46] S. Wieland, D. Bernardi, T. Schwalger, B. Lindner, Slow fluctuations in recurrent networks of spiking neurons, Phys. Rev. E 92 (2015) 1.

[47] R.F.O. Pena, S. Vellmer, D. Bernardi, A.C. Roque, B. Lindner, Self-consistent scheme for spike-train power spectra in heterogeneous sparse networks, Front. Comput. Neurosci. 12 (2018) 1.

[48] D. Cox, P. Lewis, The Statistical Analysis of Series of Events, Springer, Netherlands, 1966.

[49] N. Maier, V. Nimmrich, A. Draguhn, Cellular and network mechanisms underlying spontaneous sharp wave-ripple complexes in mouse hippocampal slices, J. Physiol. 550 (2003) 873.

[50] P. Giannopoulos, C. Papatheodoropoulos, Effects of mu-opioid receptor modulation on the hippocampal network activity of sharp wave and ripples, Br. J. Pharmacol. 168 (2013) 1146.

[51] M. Bazelot, M.T. Telenczuk, R. Miles, Single CA3 pyramidal cells trigger sharp waves in vitro by exciting interneurones, J. Physiol. 594 (2016) 2565.

[52] K. Mizuseki, G. Buzsaki, Preconfigured, skewed distribution of firing rates in the hippocampus and entorhinal cortex, Cell Rep. 4 (2013) 1010.

[53] A. Peyrache, N. Dehghani, E.N. Eskandar, J.R. Madsen, W.S. Anderson, J.A. Donoghue, L.R. Hochberg, E. Halgren, S.S. Cash, A. Destexhe, Spatiotemporal dynamics of neocortical excitation and inhibition during human sleep, Proc. Natl. Acad. Sci. USA 109 (2012) 1731.

[54] R. Brette, W. Gerstner, Adaptive, exponential integrate-and-fire model as an effective description of neural activity, J. Neurophysiol. 94 (2005) 3637.

[55] G. Maimon, J.A. Assad, Beyond Poisson: increased spike-time regularity across primate parietal cortex, Neuron 62 (2009) 426.

[56] Y.Y. Mochizuki, et al., Similarity in neural firing regimes across mammalian species, J. Neurosci. 36 (2016) 5736.

[57] M. Lundqvist, A. Compte, A. Lansner, Bistable, irregular firing and population oscillations in a modular attractor memory network, Plos Comput. Biol. 6 (2010) 1.

[58] C.A. van Vreeswijk, H. Sompolinsky, Irregular activity in large networks of neurons, in: C. Chow, B. Gutkin, D. Hansel, C. Meunier, J. Dalibard (Eds.), Methods and Models in Neurophysics, Vol. 80, Elsevier, Amsterdam, 2004, p. 341.

[59] F. Mastrogiuseppe, S. Ostojic, Intrinsically-generated fluctuating activity in excitatory–inhibitory networks, PLoS Comput. Biol. 13 (2017) 1.

[60] T.P. Vogels, K. Rajan, L.F. Abbott, Neural network dynamics, Annu. Rev. Neurosci. 28 (2005) 357.

[61] M. Rudolph, M. Pospischil, I. Timofeev, A. Destexhe, Inhibition determines membrane potential dynamics and controls action potential generation in awake and sleeping cat cortex, J. Neurosci. 27 (2007) 5280.